

NOVEL IMAGE PROCESSING TECHNIQUES FOR MEDICAL IMAGES DENOISING

¹Dr. Prachi Tripathi, ²Dr. PankajKr. Gupta, ³Dr. Bhaskar Gupta and ⁴Dr. Amit Kumar Agarwal¹Assistant Professor, NIET, Gr. Noida²Professor, MIET, Gr. Noida³Professor & Dean, MIET, Gr. Noida⁴Professor & Director, MIET, Gr. Noida**ABSTRACT**

Brain tumors are one of the leading causes of death, and hence it is critical to diagnose them early. MRI is the most effective diagnostic tool for detecting a tumor. However, thermal noise, temperature fluctuations, and other artifacts can generate noisy MRI scans, leading to inaccurate diagnoses. Deep learning algorithms combined with image processing techniques have aided in a variety of medical imaging tasks, including enhancing MRI images. Our work proposes a U-Net architecture with two encoder-decoder pairs for denoising MRI scans which were finely tuned on a dataset generated by injecting synthetic Gaussian noise. The model improved the Peak Signal to Noise Ratio (PSNR) from 11.90 to 30.96. The presented work also provides empirical evidence that the proposed denoising strategy enhances the prediction accuracy of brain tumors by nearly 23%. The developed denoising technique using U-Net would benefit radiologists and computer-aided diagnostic systems (CAD) in precisely diagnosing the disease by generating cleaner and clearer MRI scans.

Keywords—Image Enhancement, Denoising, U-Net, Brain Tumor, Gaussian Noise

(a) INTRODUCTION

A brain tumor is a clump of abnormal brain cells. The skull enclosing the human brain is incredibly hard and hence any development inside this tight region leads to major complications. As these tumors grow, the pressure inside the skull increases, causing brain damage. Brain tumors are classified into two different types viz. malignant (cancerous) and benign (noncancerous). These tumors are further classified into primary and secondary (metastatic tumors). A primary brain tumor originates within the brain however a metastatic brain tumor develops when the cancer-causing cells spread from other organs to the brain (lungs to brain). The vast majority of primary brain tumors are not cancerous.

Medical imaging is a method and procedure used to view and create visual picturization of the body for clinical and therapeutic purposes and provides a clear representation of the function of certain internal organs or tissues. Therefore, it plays an essential role in improving public healthcare for various groups of people. Medical images actually helps to reveal the hidden structures of the skin and bones, in order to diagnose diseases. It is part of biological imaging and helps in establishing a database of common body structure of humans and physiology for the discovery of abnormalities. Includes imaging technology X-ray radiography [1], magnetic resonance imaging, medical ultrasonography, elastography, endoscopy, thermography, tactile imaging, medical imaging and positron emission tomography (PET), Single-photon emission computed tomography also known as SPECT which is a technique used in nuclear medicine. Since many repetitive patterns exist in natural and medical imaging, the NLM filter proposed by it has attracted special attention to audio output especially MR images. Traditional MRI denoising techniques were originally designed to remove Gaussian noise from an image. Later new methods were proposed as non-native (NLM) methods, wavelets In this paper, we proposed an overview of different image modes, sound types and their filtering methods and discussed the removal of various sounds in MR images using different filters.

The tenth leading cause of mortality is a brain tumor. In 2020, an estimated Globally, 251,329 people died from primary malignant brain and central nervous system (CNS) tumors in 2020. In the United States today, an estimated 700,000 persons are affected with a primary brain tumor. These tumors can be deadly and have a significant impact on quality of life. Women are somewhat more likely than men to get any type of brain or spinal cord tumor, whereas men are slightly more likely to acquire a malignant tumor. This is mostly owing to the fact that some types of tumors are more prevalent in one gender or the other (for example, meningiomas are more common in women). The 5-year survival rate for those with a malignant brain or CNS tumor in the United States is 36% and only 31% when it comes to 10-year survival rate, making it a concerning condition.

Magnetic resonance imaging (MRI) [1] is commonly used to diagnose brain cancers. An MRI uses magnetic fields to generate comprehensive images of the body and can be used to evaluate tumor size. Before the scan, a specific dye known as a contrast medium is given to the patient in order to provide a crisper image. This dye is administered either through a patient's vein or orally in the form of a pill or drink. MRIs are the primary tool for

identifying a brain tumor because they give more detailed pictures than CT scans. However, in certain cases, computed tomography (CT) and positron emission tomography (PET) are utilized to detect brain tumors. The MRI may be of the brain, spinal cord, or both, depending on the type of tumor suspected. A number of specialized MRI scan components, viz. functional MRI, perfusion MRI, and magnetic resonance spectroscopy assist a radiologist in evaluating the tumor and, as a result, planning the treatment protocol.

MRIs are quite useful in detecting brain malignancies. As a result, they must be clear and precisely reflect the interior anatomy of the brain. This, however, is not the case. Noise, such as Gaussian or Rician, can contaminate MRI images, resulting in inaccurate diagnosis and hampered quantitative imaging on MRIs. A variety of sources can cause noise in an MRI. The MR machine has inherent noise induced by the thermal factor. Another consideration is the patient who is receiving the MRI scan. Thermal noise might be generated while the subject moves within the machine. Furthermore, the patient's body temperature might cause noise since lengthy exposures within MR equipment can raise the body temperature. Hence, MRI denoising becomes a critical pre-processing step when working with MRI scans.

To denoise MRI images, several image processing algorithms have been developed and used in the past. However, the denoising performance on MRI or CT images has greatly improved with the introduction of deep learning algorithms. This paper presents a U-Net [2] with two encoder-decoder pairs for MRI scan denoising. The proposed architecture was trained on 1214 noisy MRIs and obtained a peak signal to noise ratio (PSNR) of 30.96. Furthermore, the classification accuracies (whether a brain MRI has a tumor) for noisy and denoised MRI images were evaluated by training numerous state-of-the-art architectures such as DenseNet201 [3], ResNet101 [4], InceptionV3 [5], EfficientNetB7 [6], and VGG16 [7]. The proposed denoising technique improves the overall classification accuracy by 23.02%.

The BM3D is generally considered to be the best at removing noise from an image, Burger et al. [1] demonstrated how similar denoising performance can be achieved with a plain multi-layer perceptron also known as MLP. Denoising auto-encoders are the latest addition to audio removal books. They are used as a blockchain to build deep networks, which is delivered by Vincent et al, as an prior extension to the classic automatics. It was briefly shown that the default auto encoders can be packed to build a deep neural network.

The output of image produced using convolutional neural networks was a research work done by Jain et al [2]. He has proven that usage of small sample training datasets shows better performance than the usual wave fields and Markov stadiums. Agostenelli et al. [3] works with deep neural networks with many flexible columns to produce an image. With different audio images, this program shows excellent results. In Jain and Seung [4] (2008), a new image was described, describing an algorithm based on a common neural network, equivalent to the Markov Random Field (MRF) model and the multi-layer view used successfully in image extraction.

The algorithm for analyzing the new image with advanced convolutional neural networks with vision loss was largely focused on the research work done by Shan Gai. The image extraction based on the gaussian filter contains clear details of BK Shreyamsha's research work [5].

The use of a two-dimensional filter for image removal has been the main focus of Bonsle's work [6]. More detailed research work can be found in Barash's research work based on the basic relationships within dual filter, flexible, and indirect smoothing distribution rates [7].

The amount of differential filtering [8] and the filtering of non-native methods [9] [10] in medical imaging have been the field of extensive research competing with emerging algorithms such as BM3D [11].

Small image extraction and effects of [12] Gaussian-Poisson sound in very small images and their removal using a 2D wavelet algorithm [13] and a new sparsity-based approach

1. Are well discussed by Meiniel and Williams in their research work.

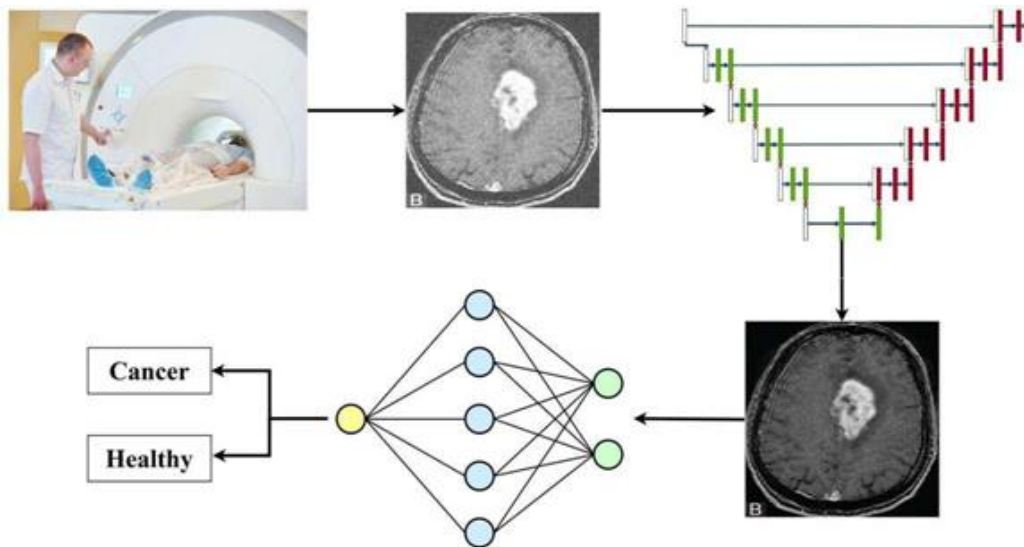


Fig. 1 Concept diagram of the developed solution. Scans generated from MRI machines are passed through the U-Net architecture. The noisy MRI is then processed by the model which gives a denoised MRI scan as an output. The denoised MRI can then be fed to a neural network to classify whether the patient has a tumor or not.

The concept diagram of the proposed system can be seen in Fig 1. It demonstrates how the proposed work can be used in a real-time clinical setting.

• LITERATURE REVIEW

Previous effort to denoise MRI pictures in the literature includes applying various image processing techniques and employing deep neural networks. When it comes to denoising an MRI picture, image processing techniques have shown tremendous results. J. Manjon et al. [8] suggested two methods for the 3D denoising MRI images. These techniques are based on a moving window discrete cosine transform hard thresholding (ODCT3D) and a 3D rotationally invariant non-local means filter (PRI-NLM3D). The ODCT3D method exploits the sparseness (high compressibility) of the MRI data, allowing for efficient noise reduction, whereas the PRI-NLM3D method exploits the sparsity by using prefiltered ODCT3D data, as well as the increased number of redundant patterns present when using a rotationally invariant non-local means filter. The PRI-NLM3D outperformed other state-of-the-art approaches for MRI denoising in the literature. Both algorithms are feasible, with less than one minute execution times, and hence can be deployed in a clinical setting. S. Hyder Ali et al. [9] proposed a curvelet-based method for denoising MRI pictures and computed tomography (CT) scans with white, random, and Poisson noise. CT scans with random gaussian noise, and MRIs with Rician and speckle noise with a factor of 30 were used. The curvelet approach at the finest scale with four decomposition levels, complex block thresholding, and cycle spinning was used to achieve superior image denoising. The curvelet transform outperformed the wavelet transform in terms of picture edge expression, such as geometric curve and beeline properties. On MRI and CT images, the suggested method produces higher peak signal-to-noise ratio (PSNR) values over a variety of underlying noise levels.

In the past few years, with the advent of neural networks, deep convolutional networks have surpassed state-of-the-art classical image processing approaches in numerous visual recognition tasks. These CNN architectures have demonstrated computational efficiency and promising outcomes when it comes to denoising MRI scans. J. Manjon et al. [10] present a hybrid strategy for noise reduction in MRI images that combines deep learning architectures with traditional approaches. First, a convolution neural network (CNN) eliminates the noise. This is done blindly, without estimating the degree of local noise in the scans. Post this step, a filtered image is then employed as a reference image within a rotationally invariant non-local means framework. The proposed CNN's input and output are 3D patches with dimensions of 12x12x12. The network contains 779,009 trainable parameters and has been trained for 100 epochs with a batch size of 128 patches. The proposed method works effectively to remove the Gaussian and Rician noise. Because of its adaptive patch-based structure, it can also deal with spatially variable noise. Tripathi et al. [11] proposed a convolutional neural network-based encoder-decoder architecture to remove Rician noise from MRI scans. The encoder structure includes two convolution and down-sampling layers, four residual blocks, and two de-convolutional layers that up-sample the residual block output. In the sampling layers, the scale factor was 2. The noisy images training dataset was generated artificially by adding Rician noise to real MRI scans.

The presented system's performance was evaluated using one stimulated and four real-world MRI datasets. The peak signal to noise ratio (PSNR) and structural similarity index (SSIM) was used in the performance analysis. In medical imaging, more radiation leads to clearer images; however, in Medical Resonance Imaging (MRI), Computer Tomography (CT), and other procedures, less radiation is applied to reduce the patient's exposure to potentially dangerous rays, resulting in noisy and low-resolution images. Gondara et al. [12] suggested a solution to this problem by employing stacked autoencoders to reduce noise in medical photos. The proposed autoencoder model was trained on the mini-MIAS dataset and the Dental radiography database (DX), consisting of 322 and 400 images, respectively. The images of the datasets were corrupted using Gaussian and Poisson noise. The Convolutional autoencoder outperformed other denoising methods like NL means and Median filter by a large margin.

O. Ronneberger [2] introduced the U-Net, a CNN network that consists of a contracting path for context capture and a symmetric expanding path for precise localization. J. Cui et al. [13] proposed an unsupervised deep learning-based approach for denoising PET scan images. The network structure was a modified 3D U-Net with bilinear interpretation layers in place of the deconvolution layers and convolution layers in place of the pooling layers. Datasets for F-FDG PET/MR and Ga-PRGD2 PET/CT were used to assess the proposed model. In comparison to denoising techniques like Gaussian, anatomically guided NLM, BM4D, and Deep Decoder, the model outperformed them.

Deep neural systems based on CNN are commonly employed in medical classification tasks. This is because they are powerful feature extractors, therefore, using them to classify medical pictures can avoid complicated and expensive feature engineering. They have been used extensively to classify MRI brain scans into different classes and for different use cases. H. A. Khan et al. [14] presented a convolutional neural network approach along with image processing and data augmentation to classify the MRI scan of the brain as cancerous or non-cancerous. The dataset consisted of 253 MRI images, of which 155 images were malignant tumors, and 98 were non-cancerous tumors. The images were preprocessed using the Canny edge detection method to identify the edges in the brain scan. The dataset was augmented using techniques like flipping, rotation, or adjusting brightness. The proposed CNN model achieved 96% training, 89% validation, and 100% testing accuracy and outperformed other state-of-the-art pre-trained models like VGG-16, ResNet-50 and Inception-V3. The major shortcoming of this work is that it is trained on a very small dataset; hence it may perform poorly in real-world data, which usually has noise, artifacts and other anomalies. J. Paul et al. [15] present two types of neural networks to classify brain MRIs into meningioma, glioma, and pituitary. In the proposed work. 989 axial images from 191 patients were used to train the deep learning architectures. Further tests were performed on augmented data. The neural networks trained over the axial images achieved an average five-fold cross-validation accuracy of 91.43%. Meningioma tumors were tough to classify, with accuracy and recall of 0.84 and 0.74, respectively, but glioma and pituitary had precision and recall in the mid-90s.

1. DATASET PREPROCESSING

In the presented work, a brain tumor dataset consisting of 253 MRI scans that were acquired from Kaggle Repository. The dataset comprises 155 MRI scans that have a brain tumor and 98 non-malignant MRI scans. The images were subjected through several preprocessing steps described below.

A. Resizing

Resizing is a pre-processing step used in computer vision to create equal-sized pictures from raw input images. Since the images obtained from the dataset were of various sizes, they were transformed into 320 by 320-pixel square monochromatic images to make them consistent throughout.

B. Dataset Augmentation

The size of the dataset is enlarged by employing techniques such as random rotation, shifting, shearing, color transformation, and flipping. In this research six-fold augmentation of the training data was carried out by flipping and rotating the original images. The images from the dataset were rotated by an angle of 15 degrees towards the left and right sides. After that, the original images were horizontally flipped and again rotated by 15 degrees to the left and right hand. The 253 images were therefore transformed into a total of 1518 images, 1214 of which served as training images. The model was tested with the final 304 images. The dataset also includes 930 samples of a brain tumor and 588 samples of normal brain images. Fig. 2 represents the data augmentation performed on a single image in the dataset.

C. Noise Injection

In medical imaging, low light conditions and movement of parts inside the imaging equipment led to degradation of the scans and increases the influence of noise on the resultant images, which in turn leads to poor

information extraction by the radiologist, leading to false diagnosis. Since multi-sensor imaging technologies are widely available, images from different sensors can be easily fused together to capture nuanced information into a single image. But a noisy scan, however, hampers the fusion of multiple subsequent images. MRIs and CT scans make use of radiation for extracting deeper features in the scans; the higher the amount of radiation, the clearer the scans. But the amount of radiation is limited to reduce the patient's exposure to harmful rays. Electronic interferences in the receiver circuits and the measurement chain of MRI scanners, i.e., coils, electronic circuits, etc., are the principal causes of noise in MRI imagery.

Noise is commonly characterized as a random variation in brightness or color information caused by poor environmental conditions. There are four main types of noise [15], Gaussian Noise, Salt and Pepper Noise, Speckle Noise, and Poisson Noise. The most common statistical noise is Gaussian noise; it follows the probability density function of normal distribution. Salt and pepper noise is a sort of noise that is typically visible in photographs. It appears as white and black pixels at random intervals. The corrupted pixels are alternately set to the lowest and highest value, creating a "salt and pepper" effect in the image. Speckle noise is multiplicative noise; it degrades image quality by giving images a backscattered wave appearance, making it difficult to detect finer details. The statistical character of electromagnetic waves, such as x-rays, gamma rays, etc., causes Poisson noise, resulting in spatial and temporal randomness in the image. Each type of noise has some specific pattern or probabilistic properties.

A dataset of noisy MRIs was developed to imitate MRI scans produced using various noise-producing factors such as sensor noise or temperature fluctuation. The dataset was constructed by introducing random noise into 1518 MRI images. Several noise intensities were applied and evaluated before picking the optimal intensity for constructing the dataset. The images produced using gaussian noise with a mean value of 0.25 were the most similar to noisy MRI scans produced during a clinical setting.

1. GAUSSIAN FILTER

Two dimensional digital Gaussian filter can be defined as[5] shown in eq(1).

$$G(x, y) = \frac{1}{2\pi\sigma^2} e^{-\frac{x^2 + y^2}{2\sigma^2}} \text{----(1)}$$

G(x y) – Output obtained from Gaussian Kernel formula, that forms part of the Kernel, which represents one object. π - Fixed figures are defined as 22/7.

1. This symbol simply represents the limit or value of a feature, as specified by input user.

e - Euler's number. Euler's numerical value is defined as a statistical value which is numerically 2.7182818284.

x, y – These two variables denote pixels linking within the image. y Represents a direct row and x represents a horizontal column.

2. Bilateral Filter:

Bilateral was introduced as a linear filtering method which can combine domain and range filtering [7]. The bilateral filter is defined as shown in eq(2).

$$W_p = \sum_{x_i \in \Omega} f_r(\|I(x_i) - I(x)\|)g_s(\|x_i - x\|)$$

$$I^{\text{filtered}}(x) = \frac{1}{W_p} \sum_{x_i \in \Omega} I(x_i) f_r(\|I(x_i) - I(x)\|)g_s(\|x_i - x\|), \text{ (2)}$$

And the normalisation term Wp is given as

$$\text{--(3)}$$

Where,

I^{filtered} defines output filtered image;

I is assigned input image to be filtered;

X gives coordinates of current filtered pixels; Sigma denotes windows centered in x;

And fr and gs are range kernel for smoothening variations in intensities and spatial kernel for smoothening variations in coordinates respectively.

It is edge-preserving, non-linear noise reduction filter for works by replacing the intensity of each pixel with weighted average of intensity values obtained from nearby pixels [6]. Weights are generally based on Gaussian distribution. Bilateral filter takes both spatial and intensity into consideration between a particular point and its neighbouring points unlike other filters[7]. This helps in preserving sharp boundaries while noise is averaged out.

3.Total variation (TV) :

Commonly known as *total variation regularisation* of total variation filtering, is a noise removal process based on principle that signals with excessive and possibly spurious detail having high total variation.

The rate of change in signal values can be measured accordingly with the usage of TV filter Specifically, the total variation of an N- point *Signal f(n)*, $1 \leq n \leq N$ is as described as below.

$$TV(\mathbf{x}) = \sum_{n=2}^N |x(n) - x(n - 1)|.$$

The total variation of \mathbf{x} can also be written as

$$TV(\mathbf{x}) = \|\mathbf{D}\mathbf{x}\|_1$$

where $\|\cdot\|_1$ is the ℓ_1 norm and

$$\mathbf{D} = \begin{bmatrix} -1 & 1 & & & & \\ & -1 & 1 & & & \\ & & & \ddots & & \\ & & & & -1 & 1 \end{bmatrix}$$

is a matrix of size $(N - 1) \times N$.

But the algorithm described here may converge slowly for some problems. The regularization parameter controls how much smoothing is to be performed. Larger the noise, larger the volume of parameter required.[8]

4. Wavelet denoising:

Wavelet filter command allows us to selectively emphasise or de-emphasise image details in a certain spatial frequency. It has a powerful advantage because of its ability to obtain the information like time, location, and frequency of an image simultaneously. Whereas the FT (Fourier transform) provides only the frequency information of the signal.

In fig 2, An image can be defined with M_1 rows and M_2 columns, output decomposed results in 4 quartersize images : details (ll,hl,hh) and approximation ll. Approximation figure ll can be defined as product of two low-passband filters and derives an input for upcoming decomposition level. The reformation is performed in the other way around i.e first on columns, then on rows. Three wavelet functions which are given as

$$\psi^1(m, n) = \phi(m)\psi(n) \text{ LHwavelet,}$$

$$\psi^2(m, n) = \psi(m)\phi(n) \text{ HLwavelet,}$$

$$\psi^3(m, n) = \psi(m)\psi(n) \text{ HHwavelet,}$$

and one scale function:

$$\phi^2(m, n) = \phi(m)\phi(n)$$

Fig 2. Wavelet denoting algorithm

5. Non Local Means (NLM):

Other than “local mean” filters which take mean value of grouped pixels around a targeted pixel towards smoothing an image, this filtering takes average value of all pixels in image according to weights relating to how similar these pixels are to target pixels. NLM can normally be classified into 4 different types , which can be used to produce better SNR value and also this is the best method for preserving edges.

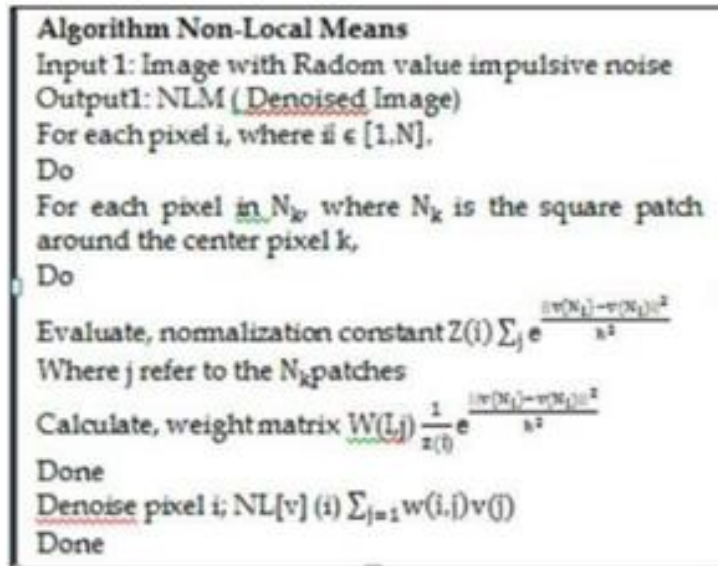
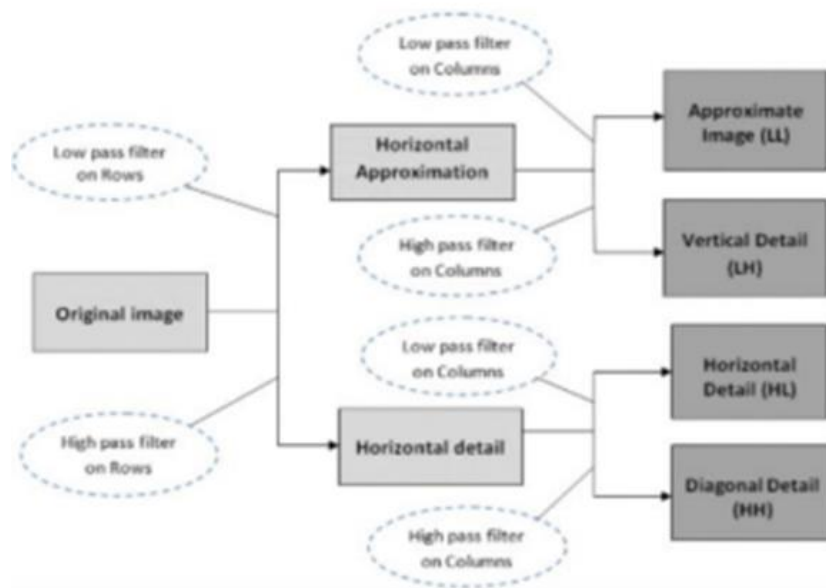


Fig 3. NLM algorithm



The general description of NLM filter can be given as[9] : When input image I is given , the filtered value at a point p which is ,the mean value of all the pixels in the image is calculated using NLM algorithm. Algorithm description is as shown in fig 3.

6. Anisotropic filter:

Filter is known for treating all axes equally. To summarize, when seen at a certain angle filter provides clarity for distant surface textures.

In image processing first anisotropic idea is dated back to Graham in 1962, followed by Newman and Dirlten , Lev , Rosefeld and Zucker

1. And Matsuyama and Mango. [10] They mainly emphasised on usage of convolutional mask that depends on the underlying image structures. Spatial regularisation strategies are usually applied in anisotropic diffusion filters.

There are two types of representations of anisotropic diffusion processes. First one shows an advantage at noisy edges, whereas second one is efficient in processing one- dimensional features.

Generally, let $\Omega \subset \mathbb{R}^2$ denotes a subset of plane and $I(\cdot, t) : \Omega \rightarrow \mathbb{R}$

be a group of gray scale images.

$I(\cdot, 0)$ is input image.

Then the anisotropic diffusion can be defined as $\frac{\partial I}{\partial t} = \text{div}(c(x,y,t)\nabla I) = \nabla \cdot (c(x,y,t)\nabla I)$ (4)

Where Δ denotes Laplacian, gradient is denoted by ∇ , and divergence operator $\text{div}(\cdot)$ and $c(x,y,t)$ is coefficient of diffusion.

Normally the results of anisotropic filters can be generalized to higher dimensions. This can be useful when considering medical image sequences from magnetic resonance imaging (MRI) or computerized tomography (CT) or while applying diffusion filters to post processing of higher dimensional numerical data.

7. BM3D

Recently, fields of interest in image processing research are non-local algorithms. In this algorithm, instead of filtering neighbourhoods, similar image blocks across image are recognised. These likely patch groups form the 3D matrix and then the obtained matrix is subjected to filtering in the transform domain with thresholds selected appropriately.

These patches have smaller equivalence of noise when compared to local neighbourhoods hence provide improved results than many neighborhood based filtering schemes.[11]

Also BM3D is known for smoothening artefacts from outputs of adaptive and median filters which appear in images with high percentage of impulses. The test image of BM3D algorithm is as shown in fig 4.

The BM3D algorithm is split into coarse and fine algorithm runs. Brief algorithm of BM3D paper can be obtained from reference paper [11].

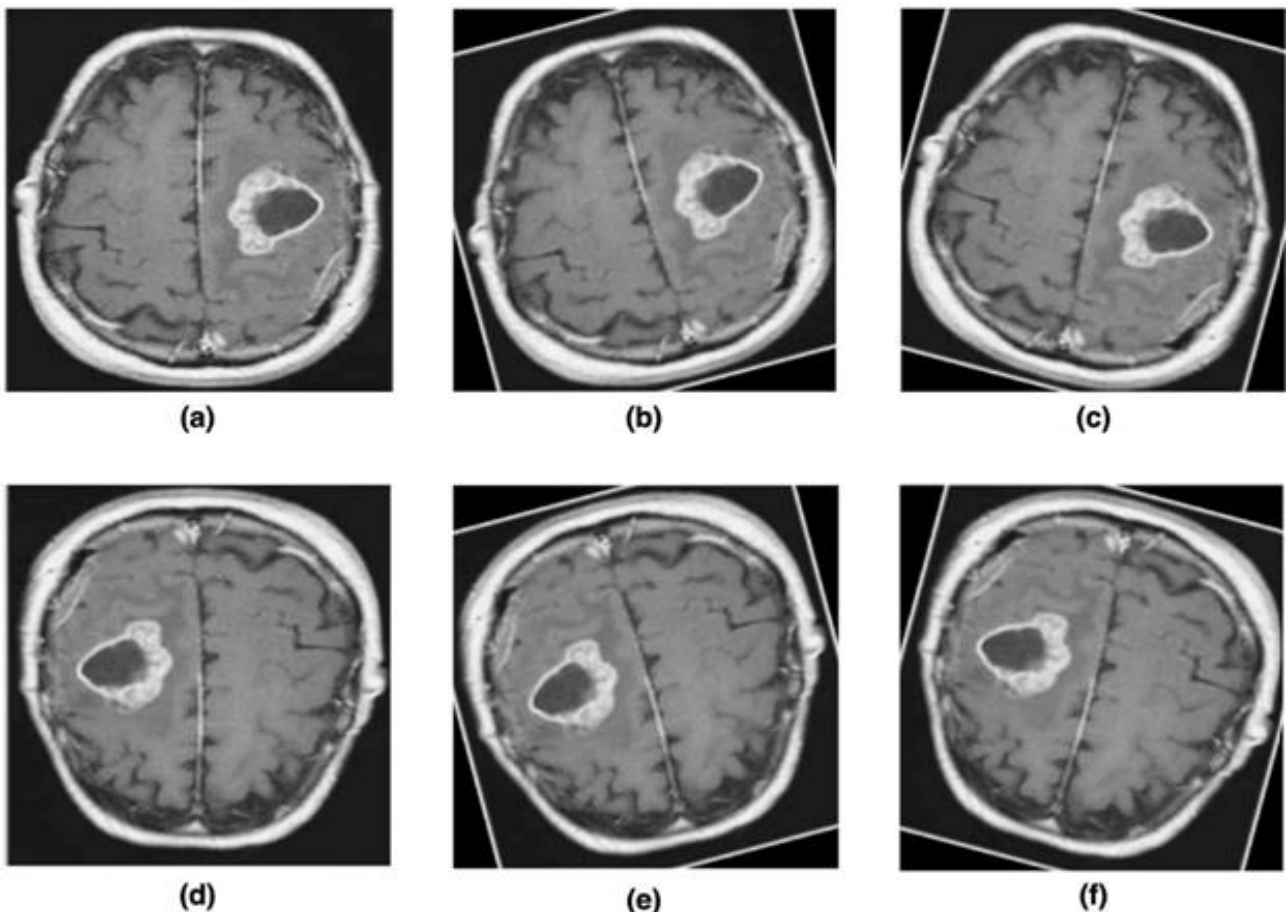


Fig. 2 Six-Fold Dataset Augmentation.

IV. METHODOLOGY

2. Denoising

For better feature extraction and classification of brain tumors, this research incorporates various techniques for the removal of the noise from the images. These include image processing methods like gaussian filtering, bilateral filtering, anisotropic diffusion and wavelet denoising. Besides image processing, this study also uses auto-encoders that fetch better results.

I. TRADITIONAL IMAGE PROCESSING TECHNIQUES:

Digital image processing is a subclass of signal processing applied to the input images to overcome the problem caused due to external distortion and noise.

- 2. Gaussian Smoothing:** Gaussian smoothing [16] or gaussian blur is an image processing method used to remove uniformly distributed noise from images using nearby pixel intensities. It is comparable to mean or average filtering. Gaussian filters, however, are inaccurate when applied to randomly distributed sounds, such as the salt and pepper noise. 2-D filters with varying sizes and weights are used for gaussian smoothing. The kernel size directly correlates with the amount of blur in the produced image. The distribution of standard deviation affects the gaussian curve as well. While increasing variance reduces noise, it also causes an increase in visual blur. Twelve different gaussian filters with standard deviations ranging from 0.01 to 5 were employed in this study. The following equation represents the gaussian distribution in the 2-D spatial domain.
- 3. Anisotropic Diffusion:** Anisotropic Diffusion is a digital image processing technique that removes noise and enhances images in 2-D or 3-D voxels. It is a very effective filtering technique used to preserve important surface features such as sharp edges and corners during the process. In a comparative study, Cesar Bustacara et al. [17] highlighted the significance of noise reduction around the edges and corners for better image classification, segmentation, smoothing, and enhancement. In this research, uniform diffusion was performed on the images since the gaussian noise present in the images was normally distributed.

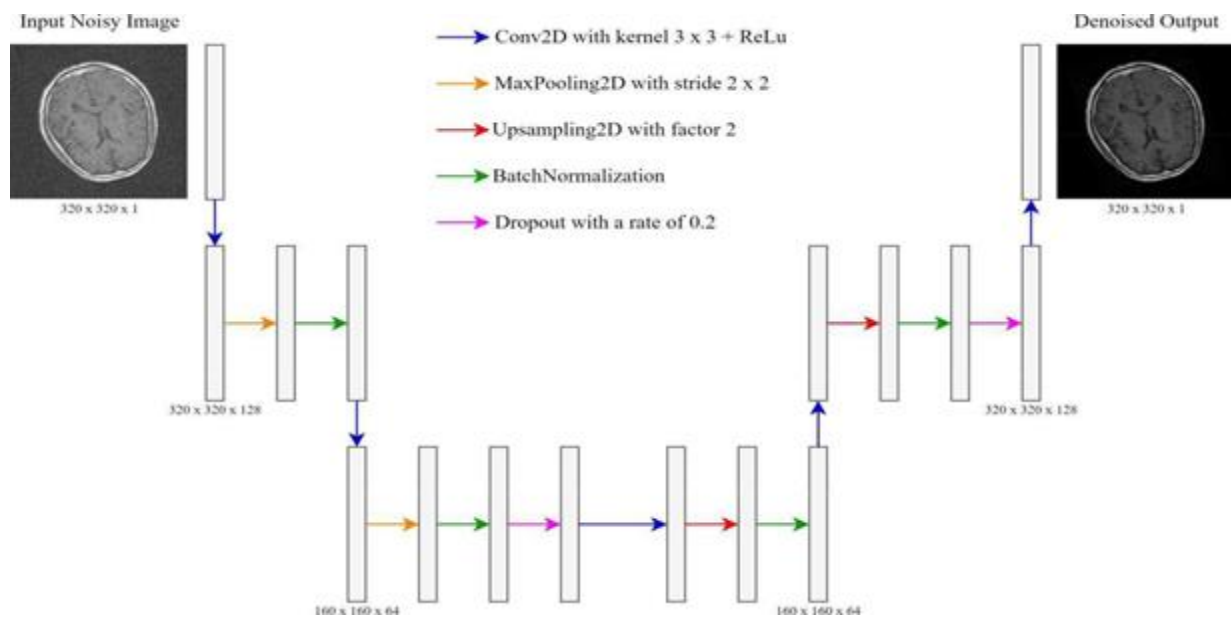


Fig. 3 The proposed U-Net architecture for denoising MRI images.

- 4. Wavelet Denoising:** Wavelet transformation [18] (WT) is another effective noise removal technique that has achieved tremendous results in denoising MRI scans. Here, the input scale is divided into many scales, each representing a separate space-frequency component of the origin signal. Some processes, such as thresholding and statistical modelling, can be conducted at each scale to suppress noise.

Bilateral Filters: The bilateral filter is an effective noise reduction method that does not sacrifice edge sharpness. In a traditional gaussian filter, the neighborhood pixels are used to calculate the gaussian weighted average. The filter is a space function and does not consider whether the pixels have the same intensity. Furthermore, it makes no distinction between whether the pixel under consideration is an edge pixel and therefore blurs the edges. However, this is not the case for bilateral filters. Bilateral filters leverage a gaussian filter in space as well as a gaussian filter that is a function of the pixel differences. The gaussian filter in space considers neighboring pixels for blurring, whereas the gaussian function that is a function of the intensity

differences ensures that the pixels with identical intensities to the center pixel are blurred, thereby preserving the edges. The presented work applied a bilateral filter with a σ_{color} value of 50 and a σ_{space} value of 50. Larger the σ_{color} , the farther the colors in the neighborhood will blend, whereas the larger the σ_{space} , the farther they will influence each other if their colors are close enough.

II. DEEP LEARNING TECHNIQUES

Autoencoders are neural networks that compress an image into lower dimensions and then use it to regenerate the image. It comprises an encoder and a decoder. The encoder is responsible for compressing the image. It generates a code which is used by the decoder to recreate the image. Both the encoder and decoder are feedforward neural networks that are fully connected.

Olaf Ronneberger et al. [2] proposed the U-NET architecture for Bio-Medical Segmentation in 2015. U-NET helps not only to classify the disease but also aids in localizing the area of anomaly. The U-NET architecture contains two sections. The first part is the reduction path (also referred to as the encoder), which is used to record the image's context. The encoder consists of stacked convolutional and max pooling layers for image size reduction to capture the low-level features in the image.

The decoder is the second half of the U-NET architecture. It semantically projects the encoder's discriminative features onto the pixel space to obtain a dense classification. Upsampling and concatenation are followed by standard convolution computations in the decoder. Different ways of upsampling include Nearest Neighbor, Bilinear interpolation, and Transposed convolution. This study employs Transposed Convolution since it delivers the most generalized and efficient upsampling of abstract representations.

In 2017, Zhengxin Zhang et al. [19] proposed a deep residual U-NET architecture for semantic or multi-class segmentation. The major shortcomings of U-NET architectures arise when the training data is limited, and additionally, they are computationally inefficient. Moreover, increasing the number of layers in the encoder leads to the vanishing gradients problem. To overcome these challenges faced by U-NET, this research also makes use of Deep Residual U-NET (RES U-NET) architecture that is infused with skip connections presented by Kaiming He et al. [20] As the name suggests, skip connections in neural networks bypass specific layers and feed the output of one layer as the input to the following levels.

The proposed U-NET architecture is represented in the Fig.

It contains two encoder-decoder blocks. The encoder block consists of a convolution layer, a max pooling layer, and a batch normalization layer. The convolutional layer is used to create an activation map of the features; the max-pooling layer is used to reduce the dimensions of the feature maps. Furthermore, the features are standardized using batch normalization. 64 and 128 unique filters are convolved within the first and second encoder blocks, respectively. To avoid overfitting, a dropout layer is added at the end of the encoder blocks that offset 20% of the neurons.

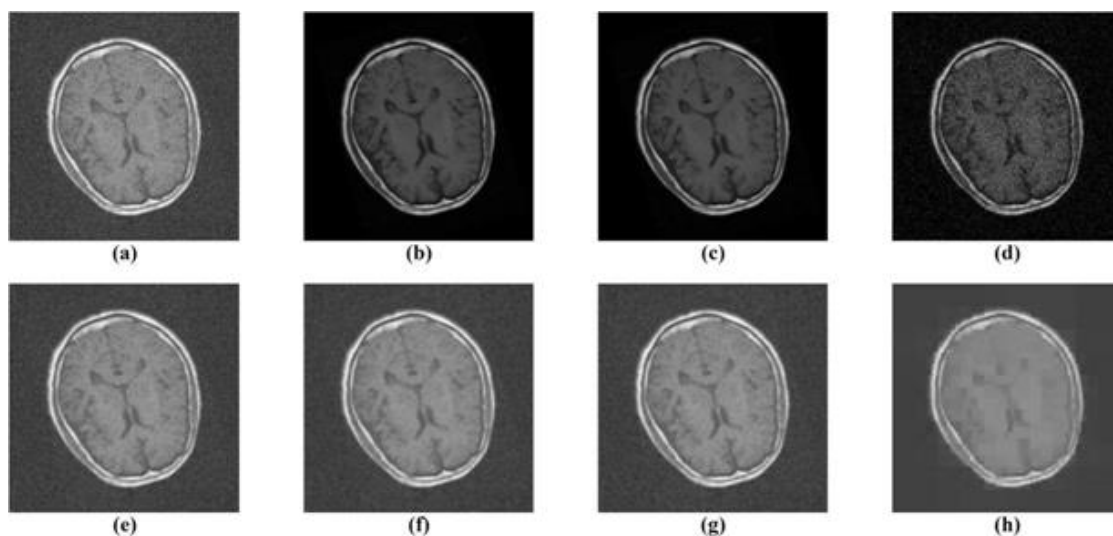


Fig. 4 Output images generated after employing different denoising strategies. (a) MRI scan after injecting gaussian noise, (b) original MRI scan, (c) denoised output from U-Net, (d) denoised output from Residual U-Net, (e) output after gaussian smoothing, (f) output after anisotropic diffusion, (g) output after applying bilateral filters, (h) output after applying wavelet denoising

The information extracted from these encoder blocks is passed to the bottleneck layer, which further extracts features before upsampling them.

Similar to the encoder block, the decoder block contains convolutional, upsampling, and batch normalization layers. The upsampling layer simply doubles the resolution of the input image without any change in the weights or features and is used as a generative layer. Analogous to the dropout layer after the encoder block, a dropout layer was added after the decoder block.

B. Classification

The images obtained after noise removal using the various autoencoders and image processing techniques were passed to five different state-of-the-art convolutional neural network architectures, namely, DenseNet201 [3], ResNet101 [4], InceptionV3 [5], EfficientNetB7 [6], and VGG16 [7]. These models were employed as a backbone, and more layers were added to these base models. The last and the penultimate layer in these models are eliminated, and seven layers and a sigmoid output layer are attached to the antepenultimate layer of the model. Firstly, a Global Average Pooling layer is used as an alternative to the Flatten layer; it computes a single average value for each input channel. Next, a batch normalization layer is used to standardize the inputs for each mini-batch, followed by a dropout layer. Two fully connected dense layers with 1024 and 512 activation units are attached in succession to the dropout layer, followed by another batch of normalization and dropout layers. Finally, the sigmoid output layer predicts the input image as a malignant or non-malignant brain tumor.

In addition to the state-of-the-art architectures, we created a custom neural network model that contains 4 CONV-POOL-BN blocks in this research. These blocks are responsible for creating kernels that can extract features from the input image. As the model proceeds toward the lower blocks, it identifies more intricate and nuanced information from the images. The number of kernels trained by each convolution layer is 32, 64, 128, and 256 in each of the four blocks. After extracting all the useful features from the images, a dropout layer was added to prevent the model from overfitting. Finally, a dense layer comprising 512 neurons is added, followed by sigmoid activation used for the binary classification.

V. RESULTS

Several image-enhancing algorithms leveraging deep learning and image processing techniques were employed to denoise the MRI scans. These techniques were compared based on the Peak Signal to Noise Ratio (PSNR). PSNR is a ratio between the greatest potential value (power) to the strength of distorting noise that influences the quality of its representation. Initially, the noisy MRI scans had a PSNR value of 11.90. The deep learning techniques fared better when compared to the classical image processing techniques. Two deep learning-based architectures viz. U-Net and Residual U-Net were trained in the proposed work. The U-Net outperformed the Residual U-Net and other image processing techniques by achieving a PSNR of 27.12. A systematic comparison of different techniques can be seen in table 1. The U-Net architecture was further tweaked by varying the depth and filters to achieve a better PSNR and classification accuracy. Fig 4. represents the output denoised images employing different techniques.

Table 1 comparison of different denoising techniques along with brain tumor classification accuracies of state-of-the-art architectures

Technique	PSNR	DenseNet201	VGG16	InceptionV3	EfficientNetB7	ResNet101	CustomCNN
Noisy	11.9013	65.46	82.89	63.82	65.13	76.32	72.04
U-Net	27.1242	98.02	98.02	98.68	74.67	96.38	98.02
Res U-Net	19.9734	36.72	38.12	35.47	29.79	34.86	65.13
Gaussian Filter	12.1250	65.13	82.89	78.28	65.13	68.42	73.68
Anisotropic Diffusion	12.1401	65.13	83.55	78.62	65.13	67.43	82.24
Bilateral Filters	12.1344	65.13	83.22	79.28	65.13	68.09	77.30
Wavelet Denoising	12.0870	65.13	84.21	77.30	64.80	65.78	70.39

Several U-Net architectures with a depth ranging from 2 to 6 were trained on the noisy MRI scans. The metrics obtained for each of these U-Nets can be seen in table 2. It can be observed that the PSNR value of the U-Net

decreased with an increase in depth. Additionally, it can also be observed that the binary image classification of brain tumor increases, which implies that the minute details of the images are not degrading. The U-Net with two encoder-decoder pairs achieved the best result with a PSNR value of 30.96. The denoised MRI images from this U-Net were passed to several convolution neural networks to classify whether the MRI scan showed signs of a brain tumor or not. DenseNet201 [3], ResNet101 [4], InceptionV3 [5], EfficientNetB7 [6], VGG16 [7] and the custom CNN architecture achieved a classification accuracy of 99.34%, 98.35%, 100%, 75.98%, 100%, and 98.68% respectively. On further analysis, it can be seen that the classification accuracy improved with an average of 23.02% for every architecture after denoising the images with the help of auto-encoders.

Table 2 comparison of different u-net variants based on depths along with brain tumor classification accuracies of different architectures

Depths of U-Nets	PSNR	DenseNet201	VGG16	InceptionV3	EfficientNetB7	ResNet101	CustomCNN
2	30.961	99.34	98.35	100	75.98	100	98.68
3	27.1242	98.02	98.02	98.68	74.67	96.38	98.02
4	23.1013	86.84	95.72	87.17	73.68	83.88	86.18
5	19.6151	79.27	88.48	76.31	69.07	69.73	68.42
6	17.8673	80.59	71.38	55.59	67.1	66.44	65.13

VI. CONCLUSION

Brain tumors are an extremely lethal malady and are the tenth leading cause of death globally, hence early diagnosis of brain tumors is critical. MRI scans of the brain are corrupted due to several noise sources. This research explores several strategies for denoising MRI images, such as auto-encoders, U-NETs, Res U-NETs, and conventional image processing algorithms, which assist radiologists in making more precise judgments. The work reported here offers a novel and optimal solution to this problem, and the proposed system outperformed existing state-of-the-art methods.

REFERENCES

1. Vlaardingerbroek, Marinus T., and Jacques A. Boer. *Magnetic resonance imaging: theory and practice*. Springer Science & Business Media, 2013.
2. Ronneberger, Olaf, Philipp Fischer, and Thomas Brox. "U-net: Convolutional networks for biomedical image segmentation." *International Conference on Medical image computing and computer-assisted intervention*. Springer, Cham, 2015.
3. Huang, Gao, et al. "Densely connected convolutional networks." *Proceedings of the IEEE conference on computer vision and pattern recognition*. 2017.
4. He, Kaiming, et al. "Deep residual learning for image recognition." *Proceedings of the IEEE conference on computer vision and pattern recognition*. 2016.
5. Szegedy, Christian, et al. "Going deeper with convolutions." *Proceedings of the IEEE conference on computer vision and pattern recognition*. 2015.
6. Tan, Mingxing, and Quoc Le. "Efficientnet: Rethinking model scaling for convolutional neural networks." *International conference on machine learning*. PMLR, 2019.
7. Simonyan, Karen, and Andrew Zisserman. "Very deep convolutional networks for large-scale image recognition." *arXiv preprint arXiv:1409.1556* (2014).
8. Manjón, José V., et al. "New methods for MRI denoising based on sparseness and self-similarity." *Medical image analysis* 16.1 (2012): 18-27.
9. Hyder, S. Ali, and R. Sukanesh. "An efficient algorithm for denoising MR and CT images using digital curvelet transform." *Software Tools and Algorithms for Biological Systems*. Springer, New York, NY, 2011. 471-480.

10. Manjón, José V., and Pierrick Coupé. "MRI denoising using deep learning." International Workshop on Patch-based Techniques in Medical Imaging. Springer, Cham, 2018.
11. Tripathi, Prasun Chandra, and Soumen Bag. "CNN-DMRI: a convolutional neural network for denoising of magnetic resonance images." Pattern Recognition Letters 135 (2020): 57-63.
12. Gondara, Lovedeep. "Medical image denoising using convolutional denoising autoencoders." 2016 IEEE 16th international conference on data mining workshops (ICDMW). IEEE, 2016.
13. Cui, Jianan, et al. "PET image denoising using unsupervised deep learning." European journal of nuclear medicine and molecular imaging 46.13 (2019): 2780-2789.
14. Pathak, Krishna, et al. "Classification of brain tumor using convolutional neural network." 2019 3rd International conference on Electronics, Communication and Aerospace Technology (ICECA). IEEE, 2019.
15. Paul, Justin S., et al. "Deep learning for brain tumor classification." Medical Imaging 2017: Biomedical Applications in Molecular, Structural, and Functional Imaging. Vol. 10137. SPIE, 2017.
16. Chung, Moo K. "Gaussian kernel smoothing." arXiv preprint arXiv:2007.09539 (2020).
17. Number 1 here
18. Debnath, Lokenath, and Firdous Ahmad Shah. Wavelet transforms and their applications. Boston: Birkhäuser, 2002.
19. Zhang, Zhengxin, Qingjie Liu, and Yunhong Wang. "Road extraction by deep residual u-net." IEEE Geoscience and Remote Sensing Letters 15.5 (2018): 749-753.
20. He, Kaiming, et al. "Deep residual learning for image recognition." Proceedings of the IEEE conference on computer vision and pattern recognition. 2016.
21. L. Gondara, "Medical Image Denoising Using Convolutional Denoising Autoencoders," 2016 IEEE 16th International Conference on Data Mining Workshops (I C D M W) , 2016 , pp. 241 - 246 , doi: 10 . 1109 / ICDMW.2016.0041.
22. Deng Jia et al. "Imagenet: A large-scale hierarchical image database" Computer Vision and Pattern Recognition 2009. CVPR 2009. IEEE Conference on. IEEE 2009.
23. Agostinelli Forest Michael R. Anderson and Honglak Lee "Adaptive multi-column deep neural networks with application to robust image denoising" Advances in Neural Information Processing Systems 2013.
24. Jain Viren and Sebastian Seung "Natural image denoising with convolutional networks" Advances in Neural Information Processing Systems 2009.
25. Kumar, BK Shreyamsha. "Image denoising based on gaussian/ bilateral filter and its method noise thresholding." Signal Image Video Process. 7.6 (2013): 1159-1172.
26. Bhonsle, Devanand, Vivek Chandra, and G. R. Sinha. " Medical image denoising using bilateral filter." International Journal of Image, Graphics and Signal Processing 4.6 (2012): 36.
27. Barash, Danny. "Fundamental relationship between bilateral filtering, adaptive smoothing, and the nonlinear diffusion equation." IEEE Transactions on pattern analysis and machine intelligence 24.6 (2002): 844-847.
28. Selesnick, Ivan W., and Ilker Bayram. "Total variation filtering." White paper (2010).
29. Manjón, J. V., Carbonell-Caballero, J., Lull, J. J., García-Martí, G., Martí-Bonmatí, L., & Robles, M. (2008). MRI denoising using non-local means. Medical image analysis, 12(4), 514-523.
30. Weickert, Joachim. Anisotropic diffusion in image processing. Vol. 1. Stuttgart: Teubner, 1998.

31. [Djurović, Igor. "BM3D filter in salt-and-pepper noise removal." EURASIP Journal on Image and Video Processing 2016, no. 1 (2016): 1-11.
32. Benoit B. "A fast fractional Gaussian noise generator." *Water Resources Research* 7.3 (1971): 543-553.
33. Debashis Ganguly, Srabonti Chakraborty, Maricel Balitanas, and Tai-hoon Kim," Medical Imaging: A Review" International Conference on Security-Enriched Urban Computing and Smart Grid, SUComS 2010
34. Sugandha Agarwal, O.P. Singh and Deepak Nagaria, "Analysis and Comparison of Wavelet Transforms For Denoising MRI Image" *Biomedical & Pharmacology Journal* Vol. 10(2), 831-836 (2017)
35. Mohd. Ameen, Shah Aqueel Ahmed, "An Extensive Review of Medical Image Denoising Techniques", *Global Journal of Medical Research: Radiology, Diagnostic Imaging and Instrumentation*, Volume 16, Issue 2 Version 1.0, 2016
36. Rajesh Patil, S. J. Bhosale, "Medical Image Denoising Techniques: A Review", *International Journal on Engineering, Science and Technology*, Volume 4, No 1, 2022
37. S. Kother Mohideen, Dr. S. Arumuga Perumal et al. (2008), "Image De-noising using Discrete Wavelet Transform" , *IJCSNS International Journal of Computer Science and Network Security*, VOL.8 No.1
38. Kim-Han Thung, Paramesran Raveendran, "A Survey of Image Quality Measures" Conference Technical Postgraduates, Jan 2010
39. Barten P. G. J. (1999), "Contrast sensitivity of the human eye and its effects on image quality", SPIE Optical Engineering Press, Bellingham, WA .
40. Kaur chitranjanjit, kapoor pooja, kaur Gurjeet(2023), "image recognition(soil feature extraction)using Metaheuristic technique and artificial neural network to find optimal output.*Eur. Chem. Bull.*2023(special issue 6).
41. Maheshwari Chanana shalu, Kapoor pooja,kaur chitranjanjit(2023),"Data mining techniques adopted by google: A study.: *Empirical Economics Letters*,22(special issue 2).
42. Marta M., Grgic S. and Grgic M. (2003), "Picture quality measures in image compression systems", *Proceedings EUROCON '03*, p. 233-237
43. Nadir Mustafa, Jiang Ping Li et al. (2015), "Medical Image De-Noising Schemes using Wavelet Transform with Fixed form Thresholding", (*IJACSA*) *International Journal of Advanced Computer Science and Applications*, Vol. 6, No. 10
44. R. Sujitha, C. Christina, De Pearlin et al. (2017), "Wavelet Based Thresholding for Image Denoising in MRI Image" *International Journal of Computational and Applied Mathematics*. ISSN 1819-4966 Volume 12, Number 1
45. Ajeet Singh (2013), "Denoising of Medical Images Using Wavelet Transform",*International Journal of Scientific & Engineering Research*, Volume 4, Issue 7, July-2013
46. Marwa Chafii, Jacques Palicot, Rémi Gribonval (2017), "Wavelet modulation: An alternative modulation with low energy consumption", *C. R. Physique* 18 pg. 156-167
47. Kumar N, Alam K, Siddiqi A. H. Wavelet Transform for Classification of EEG Signal using SVM and ANN. *Biomed Pharmacol J* 2017;10(4).
48. S. Behzadpour et al., "Multiresolution wavelet analysis applied to GRACE range-rate residuals", *Geosci. Instrum. Method. Data Syst.*, 8, 197–207, 2023